Evaluation of X22CrMoV12-1 Alloy with Vanadium Carbide Addition Submitted to Powder Metallurgy

Roberta Alves Gomes Matos[a]* (ID)*, Jonas Mendes[a], Bruna Horta Bastos Kuffner[a]* (ID)*,*

Mirian de Lourdes Noronha Motta Melo[a] (ID)*, Gilbert Silva[a]* (ID)

[a]Universidade Federal de Itajubá (UNIFEI), Itajubá, MG, Brasil.

Usually, scraps of X22CrMoV12-1 alloy are obtained through machining of steam turbine blades and recycled through casting. However, this process is considered too costly. The viability of recycling X22CrMoV12-1 scraps with addition of vanadium carbide (VC) through powder metallurgy was analyzed in this study. Scraps of X22CrMoV12-1 alloy with VC were milled in a planetary ball mill during 10, 30 and 60 hours. The granulometry of the powder was determined through laser granulometry. The evolution in particles morphology and amorphization was conducted using scanning electron microscope (SEM) and x-ray diffraction (DRX) techniques. Stress-strain curves were obtained through compressive strength test. The results indicated that the best milling condition found was 60 hours. Also, the X22CrMoV12-1 alloy with VC addition produced by powder metallurgy showed good mechanical strength. Thus, this route was considered promising to reshape this material with smaller energy involved in the process.

Keywords: *X22CrMoV12-1 Alloy, Carbides, High Energy Ball Milling, Powder Metallurgy, Microstructural and Mechanical Analysis.*

1. Introduction

Materials resistant to high temperature and pressure operations represent a high demand in power plants. It demands the use of different types of materials, with specific chemical compositions and microstructural and mechanical characteristics. Thus, the refinement of materials to meet these demands is stimulated, existing then a tendency to improve the properties of these materials. In general, the gases circulating inside of these systems expose the equipment to pressures and temperatures of approximately 20 MPa and 600 ºC, respectively. With this, the efficiency of steam turbines can be bettered through an increase in these parameters[1-3].

Development of high chrome (9-12%) martensitic steels has been heavily incentivized by its combination of high creep and thermal fatigue strength, corrosive resistance, low cost and good machinability[4-6].

Steels with 9-12%Cr such as the X22CrMoV12-1 are under development since 1940, with specific use in steam and gas turbine applications, as well in critical components of fossil and nuclear power plants. These materials are designed to support high working temperatures, high creep and fatigue resistances. Also, these steels must be resistant to embrittlement during the course of long-term use at high temperatures[7-9].

The creep resistance of this alloy is superior to that of ferritic steels and earlier generation martensitic steels. Due to its high microstructural stability, it is used in long operational cycles without changing its mechanical properties, even when exposed to superheated vapors. Also, the high corrosion resistance is a result of the presence of chrome (Cr), manganese (Mn) and silicon (Si) in the chemical composition of this material[10,11].

The recycling of scraps obtained from the machining of this alloy becomes interesting in face of these properties. The main recycling route is casting, process in which a substantial amount of energy is consumed. On the other hand, the amount of energy consumed in the process can be reduced significantly when the scraps are transformed in powder through mechanical milling, followed by consolidation in semi-finished products. Another way to improve the properties of this alloy is with the addition of hardening particles in the matrix during high energy ball milling. VC is an excellent hardening filling due to its high melting point (2830 ºC), hardness (2460-3150 HV), good plasticity and wettability in iron based materials[12,13].

The use of high energy ball mills dates from 1966. They used to be applied as a tool for the mechanical alloying (MA), a technique created to enhance the mechanical properties of different types of alloys. After the emergence of MA, the mechanical milling (MM) arised as an alternative route to the use of mills[14].

High energy ball milling is a process in which powders in solid state are processed, permitting the production of a variety of alloys in and out of equilibrium, starting from elementary powders by means of reducing the initial particles size. This process is composed of repeated soldering and fracturing of the powder particles, enabling the synthesis

*e-mail: ro.alves@ymail.com

of supersaturated solid solutions, metastable solutions, amorphous alloys, quasicrystalline phases, nanocomposites, nanostructured and nanocrystalline materials[15-17].

In turn, the powder metallurgy is considered an interesting manufacturing route, with great potential for use in various engineering applications. Through PM, it is possible to produce since workpieces with various shapes, up to refractory metals with high melting point. In this route, metallic or ceramic fine powders are blended, usually in ball mills, compacted inside of designed dies using hydraulic press and then, sintered using controlled atmosphere, in order to diffuse the particles in contact. All steps involved are important, once that affect the quality of the final product. Problems such as bad homogenization of powders and high porosity in the compact can imply in severe decrease in mechanical properties[18-21].

Thus, this study aimed to evaluate the microstructural and mechanical properties of the X22CrMoV12-1 alloy, initially in the form of aircraft steam turbine blade, which reached the end of its life cycle. The powder metallurgy was the route chosen to perform the recycling of this material, being the vanadium carbide (VC) used as stress-inducing hard particle in the milling process.

2. Experimental

The forerunner powders obtained in this study were produced through high energy ball milling, using machining residues (scraps) of X22CrMoV12-1 alloy with addition in weight of 3% of VC. This carbide was manufactured industrially and has an average particle size of 1 μm. The milling process was performed in a planetary ball mill, with tungsten carbide (WC) spheres, 316L stainless steel jars and atmosphere of high purity argon N5. The milling parameters used are described in Table 1.

After 60 hours of milling, the powders were sifted using a 100 mesh sieve (150 μm), and later, uniaxially compacted, inside of a 12 mm diameter matrix, with 200 MPa of press during 30 seconds, being this procedure repeated three times. 2% in weight of zinc stearate was added to the powders, as binding agent.

After pressing, the sintering in vacuum atmosphere followed according to two heating parameters. In the first, the samples were heated in a rate of 5 ºC/min up to 500 ºC, being maintained during 30 minutes, with the objective to eliminate the zinc stearate from inside of the samples, through volatilization. If a faster heating rate had been used, the samples would have exploded inside the furnace, as a consequence of the gases released. After this first step, the heating rate was increased to 10 ºC/min up to 1200 ºC,

being maintained for 60 minutes. After this procedure, the samples were cooled inside the furnace.

Subsequent heat treatments of quenching and tempering were applied, in order to enhance the mechanical properties of the material produced. For quenching, it was used a temperature of 1050 ºC during 60 min, being the samples cooled in air. For tempering, a temperature of 710 ºC during 120 min was applied, being the samples cooled in air.

The microstructural analysis of the samples produced was performed using tests of optical microscopy (Olympus® BX41M) with aid of the image analysis software Stream Basics and chemical etching using Vilella reagent with times varying from 10-50 seconds. The apparent porosity was determined based on the analysis of 5 samples, where the average of 10 different regions of each sample was obtained. Other analysis were employed, such as laser granulometry (Microtrac®), scanning electron microscopy (Carl Zeiss® EVO MA 15) in the modes secondary electron (SE) and energy dispersive spectrometer (EDS) as punctual and mapping and x-ray diffraction (Panalytical® X'Pert PRO) with voltage of 40 kV, current 40 mA, scan range of 30 to 130°, step of 0.02°/second and cobalt tube. For mechanical analysis of the samples, the compression strength was evaluated (INSTRON® 8801), with capacity of 10 tf and compression speed of 2 mm/min. The samples used presented initial dimensions of 10.8 mm of diameter and 5 mm of height. The elastic modulus (E) was obtained using the equation E = tensile stress / tensile Strain. These values were obtained from the stress-strain curves.

3. Results and Discussions

The comminution of the X22CrMoV12-1 alloy with VC addition was evaluated according to the evolution in the milling times (Figure 1). The VC was added to the milling process with the intention to contribute in the reduction of the steel particles size. This reduction in the dimension of the steel particles is associated to the high hardness of the VC, which activates the ductile-brittle milling mechanism. In this, the hard brittle particles of the ceramic material infiltrate the interlamellar spaces of the ductile steel. Thus, when the milling spheres collide with the steel under high rotation speeds, their impact induces a higher tension in the regions of the steel that possess brittle particles inserted. This phenomena accelerates the processes of cold welding, strain hardening and rupture of the ductile material. With this, after milling, the final size of the steel particles corresponds to a combination of brittle particles inserted within the steel interlamellar spaces particles[22].

Figure 1a shows the initial scraps, as received. It is observed that they present helical morphology, with approximate thickness of 2 mm. Also, there is no presence of oxidation, which indicates that the machining was performed properly. After the milling process, it is verified that after 10 hours of milling (Figure 1b), the particles presented irregular morphology, with presence of clusters. Increasing the milling time from 10 to 30 hours, the particles changed their morphology to spherical, being the clusters maintained. For 60 hours of milling, it is noted that the particles morphology remained spherical. However, it is evident that the particles had their

Table 1. X22CrMoV12-1 alloy milling parameters.

Parameter	Milling condition
Starting powders	X22CrMoV12-1 (30 g) and VC (0.9 g)
Milling speed	350 rpm
Milling times	10, 30 and 60 hours
Milling downtime	15 min/hour
Ball to powder ratio	10:1
Milling atmosphere	Ar N5 (99.9999% purity)
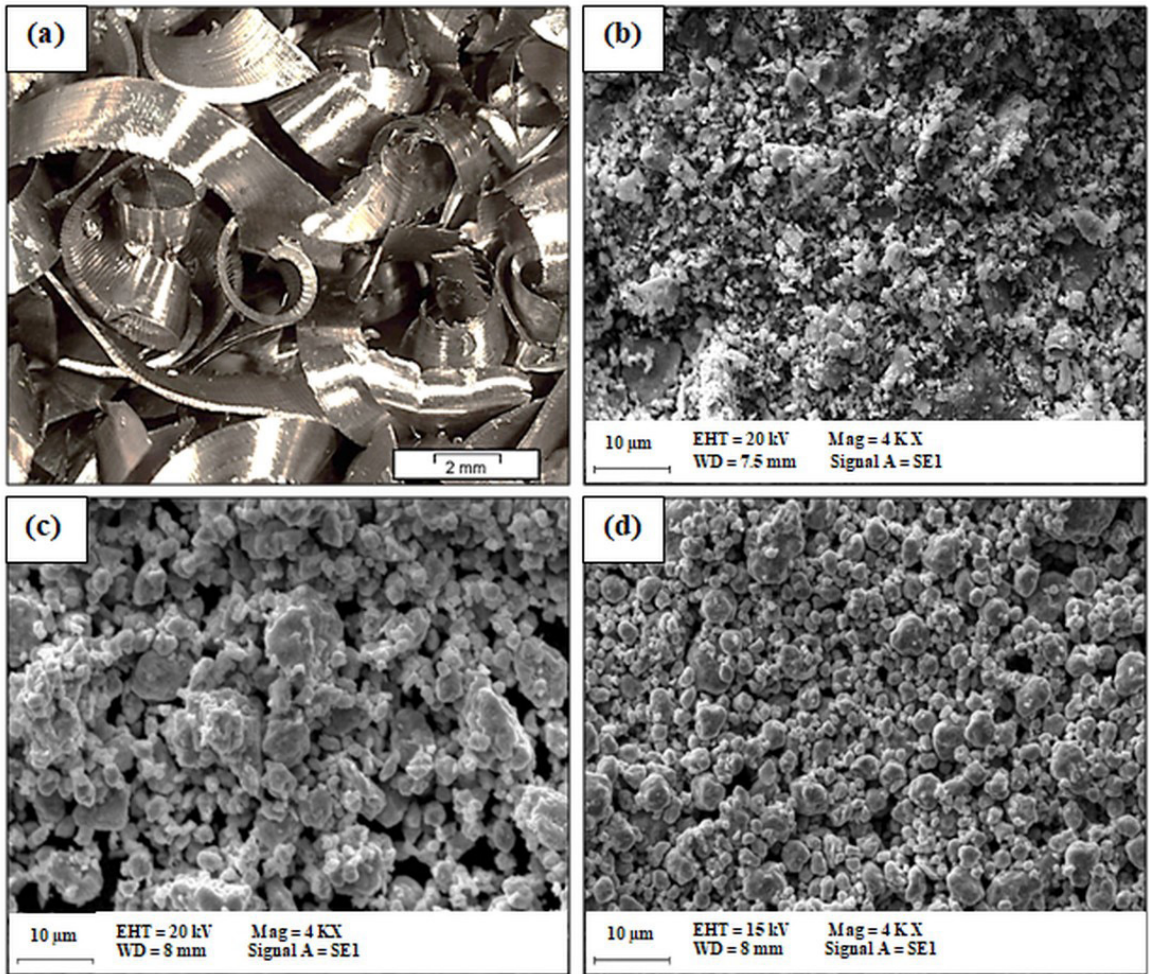
Figure 1. X22CrMoV12-1 alloy + VC SEM micrographs (a) Scraps as received (b) 10 hours of milling (c) 30 hours of milling (d) 60 hours of milling.

size reduced, as well the presence of clusters significantly decreased.

The laser granulometry results obtained for X22CrMoV12-1 alloy with VC after milling can be seen in Table 2. After 10 hours, the particles presented a higher volume (57.3%) located in a range of 10 μm, 25.3% of particles with 43 μm and 17.4% of particles with 3 μm. Increasing the milling time to 30 hours, it is noted that the distribution of particles remained practically the same than for 10 hours, with the higher volume of particles (43.5%) located in a size of 11 μm, 25.9% of particles with 54 μm and 8.2% of particles with 4 μm. The only difference observed is that the presence of cluster is more pronounced for 30 hours, since that a volume of 22.4% of particles with 160 μm was found. They are not considered as single particles, but as an agglomeration of them, which was possible to see in Figure 1c. Vallabh et al.[23] attribute the particle adhesion to either electrostatic charges acquired and distributed along the surface, or by cold welding during the milling process. Reed[24] affirms that the bonds within these agglomerates are relatively weak and are either Van der Walls forces or magnetic forces. Chang and Zhao[25] affirmed that the distribution in size

Table 2. Laser granulometry results obtained for X22CrMoV12-1 alloy + VC after milling.

| Milling Time	Particles Volume (%)	Particles Size (μm)
10 h	25.3	43
	57.3	**10**
	17.4	3
30 h	22.4	160
	25.9	54
	43.5	**11**
	8.2	4
60 h	**77.3**	**10**
	22.7	4

for particles in this phase was narrowed, once that particles bigger than the average were reduced at the same rate in which agglomerates of smaller particles were formed. For 60 hours of milling, it was observed a better evolution in the particles size, since that those in a range of 40-60 μm were no longer found. In general, the higher volume (77.3%) of particles presented size of 10 μm, as well as the volume of particles with 4 μm increased to 22.7%, the best result among all

milling conditions. It is highlighted that with the evolution in the milling time, it is possible to see that the volume of smaller particles increase, at the same time that the volume of bigger particles and clusters decrease. However, it is not possible to achieve particles with size smaller than 3-4 μm.

The semi-quantitative chemical analysis and mapping of the X22CrMoV12-1 powder with VC addition after 60 hours of milling is shown in Figure 2. It is possible to observe the distribution of the elements Fe (red points), Cr (green points), Mo (light blue points), V (dark blue points) and C (purple points), constituents of both X22CrMoV12-1 alloy and VC. As it can be seen, all of the elements are evenly distributed over the powder surface. It attests that the mechanical milling of this alloy with VC is a promising approach, once that the process not only transformed scraps in small particles, but also homogenized equally the particles of both materials together. In the graph of chemical analysis, the peaks with higher intensity are of the elements with higher volumetric fraction in the final powder, corresponding to Fe and Cr.

Figure 3 indicates the apparent porosity analysis of the X22CrMoV12-1 alloy with VC after uniaxial pressing and sintering. In Figure 3a, it is observed a micrograph via SEM of the matrix with low apparent porosity and high densification, as a consequence of a sintering with high
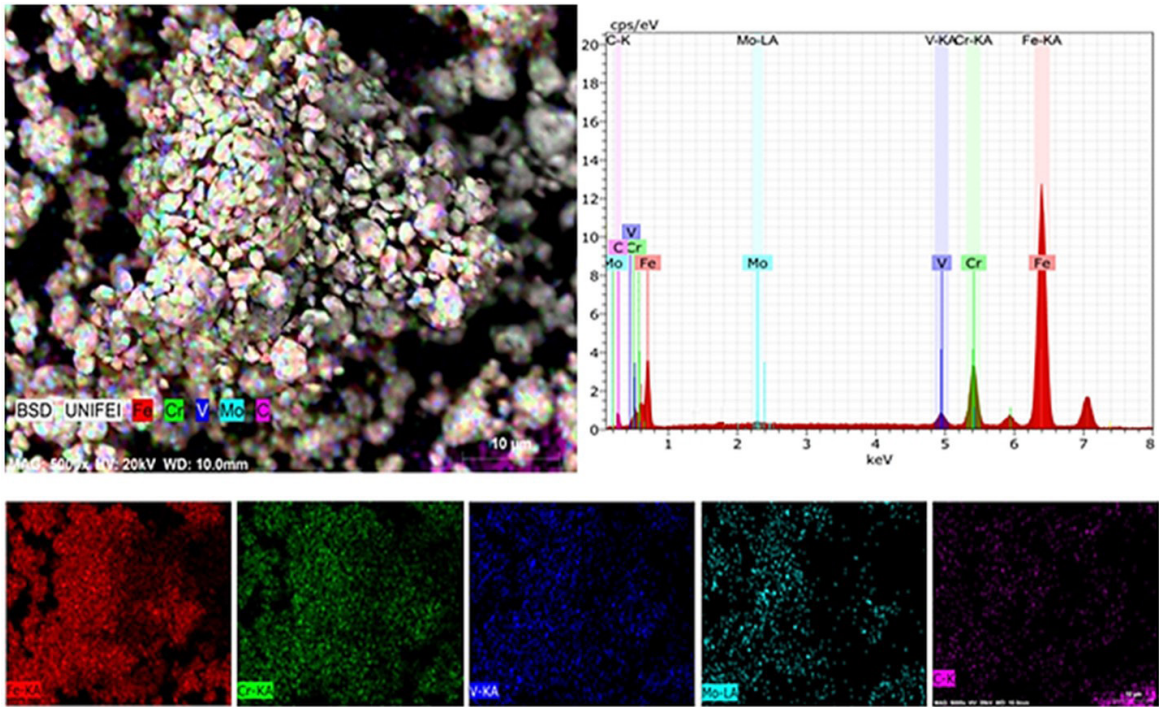
Figure 2. Semi-quantitative chemical analysis and mapping of X22CrMoV12-1 alloy with addition of VC particles after 60 hours of milling.
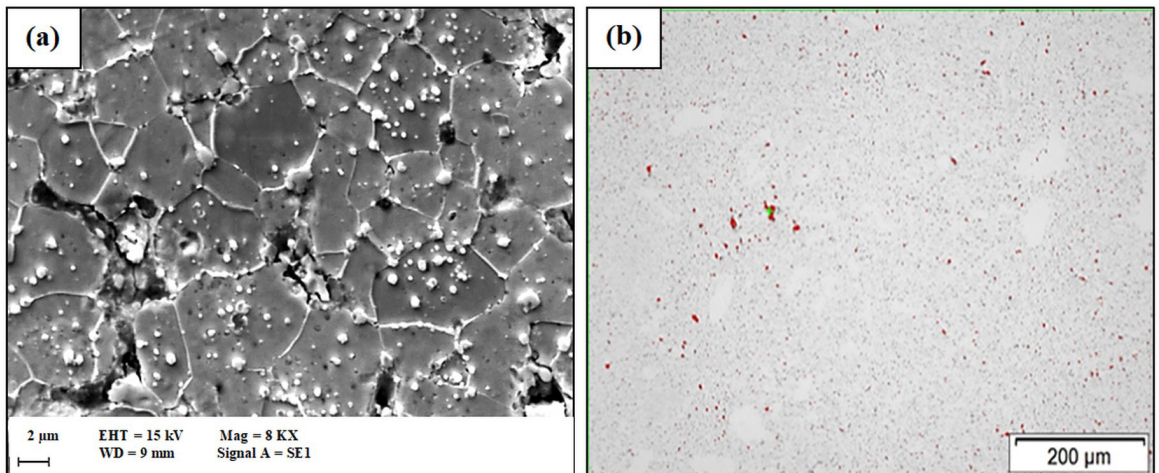
Figure 3. Microstructure of X22CrMoV12-1 alloy with VC addition after sintering (a) SEM analysis (b) OM analysis of apparent porosity.

rate of diffusion. This result is also confirmed by Figure 3b, where through optical microscopy analysis the red dots represent the apparent porosity encountered. After analysis, an average apparent porosity of 1.25% was determined. This data was obtained through optical microscopy image analysis. For this condition, the sintering process reached the third stage, in which the contraction and reduction in pore diameter occurred properly[26].

In Figure 4, the resulting microstructure after quenching and tempering was analyzed through SEM, with the emission of an electron beam. Investigations were conducted in four different points, to identify the precipitated phases in the matrix. In Figure 4a, it is possible to see a better view of matrix and precipitates, while in Figure 4b, a better view of the grain boundaries.

The EDS spectrogram with the chemical analysis and percentages of each chemical elements of Points 0 and 1 can be seen in Figures 5 and 6, respectively. Point 0 revealed a precipitate with composition containing Fe, Cr, Mo, C, Nb, Mn, V and Si, which corresponds to the Z phase (Cr(V,Nb) N). This phase can be formed during standard thermal treatment, depending on the chemical composition of the steel[27,28]. For Danielsen and Hald[29], V, Nb and Ta can form a Z phase when combined with Cr and N. This formation occurs by diffusion of Cr in MX type precipitates already existent and that present higher thermodynamic stability in temperatures between 600-650 °C than the Z phase. Also, Cr levels about 10.5% strongly accelerate the precipitation of Z phase[28-30]. As mentioned by Cipolla et al.[28], this phase is basically a CrV based nitrate, which also contains limited
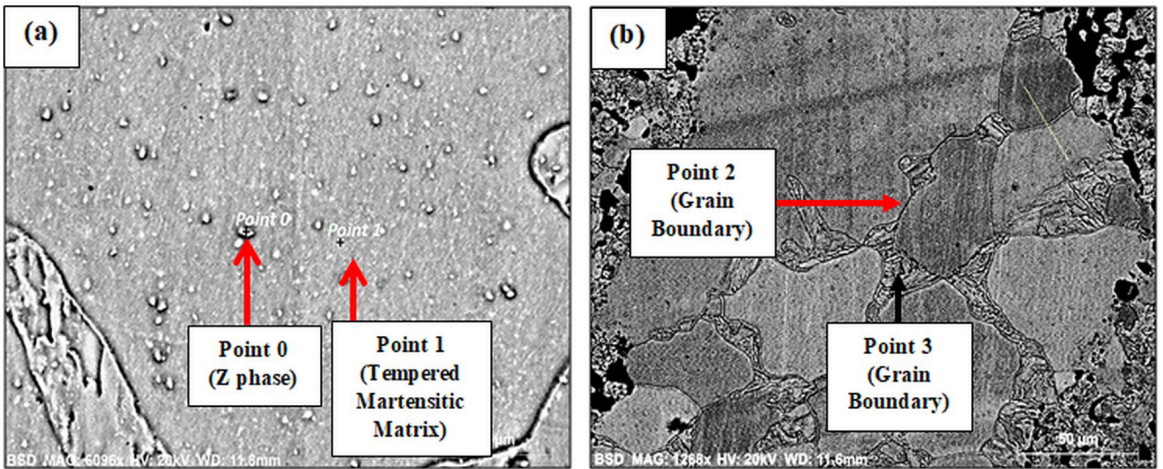

Figure 4. X22CrMoV12-1 alloy spots of chemical analysis (a) View of matrix and precipitates (b) View of grain boundaries.

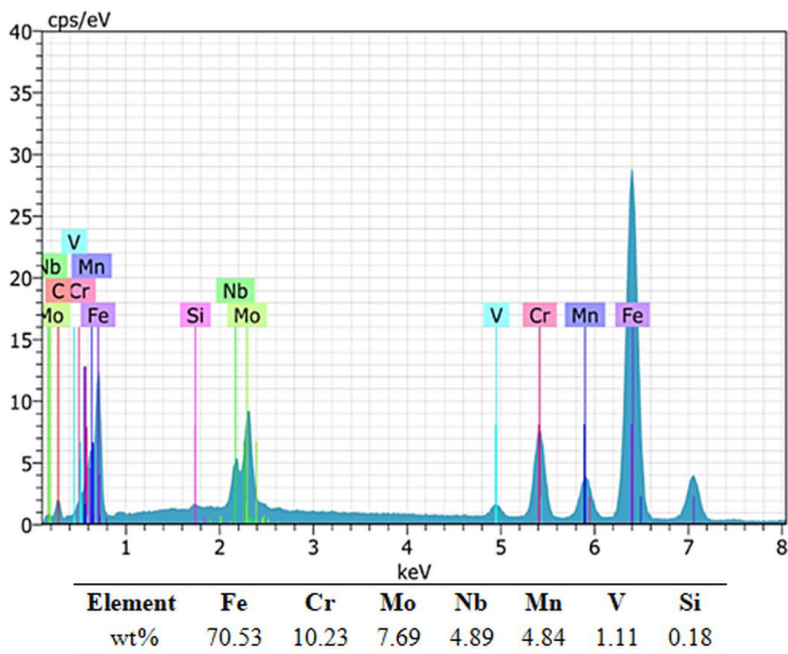| Element	Fe	Cr	Mo	Nb	Mn	V	Si
wt%	70.53	10.23	7.69	4.89	4.84	1.11	0.18

Figure 5. Spectrogram of X22CrMoV12-1 alloy in point 0.

quantities of Nb and Fe, and transforms in Z when exposed to high temperatures. Point 1 represents only chemical elements of the X22CrMoV12-1 matrix, composed by a tempered martensitic phase. It is noteworthy that the microstructure of the sintered X22CrMoV12-1 alloy is composed by a martensitic phase.

The EDS spectrogram with the chemical analysis and percentages of each chemical elements of Points 2 and 3, which correspond to the grain boundaries, can be seen in Figures 7 and 8. This analysis was performed in order to identify precipitates in these regions. After evaluation, it was noted that the composition was the same, only with a change in the volumetric fractions.

Figure 9 presents the x-ray diffractogram of the X22CrMoV12-1 alloy as casted, as powder milled with VC for 10 hours, 30 hours, 60 hours, sintered and after heat treatments. The black squares correspond to the FeCr phase, while the red circles, the Fe_4C phase. According to the ICSD database, the phases found were based on the crystallographic sheets FeCr (03-065-4607) and Fe_4C (03-065-3286). For both
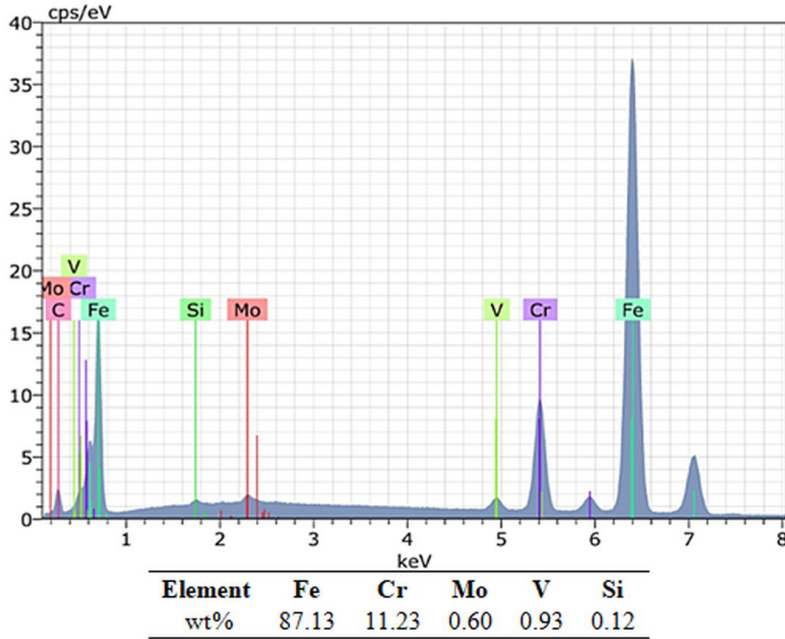

Element	Fe	Cr	Mo	V	Si
wt%	87.13	11.23	0.60	0.93	0.12

Figure 6. Spectrogram of X22CrMoV12-1 alloy in point 1.

Element	Fe	Cr	Mo	V	Si
wt%	87.24	10.98	0.57	1.07	0.13
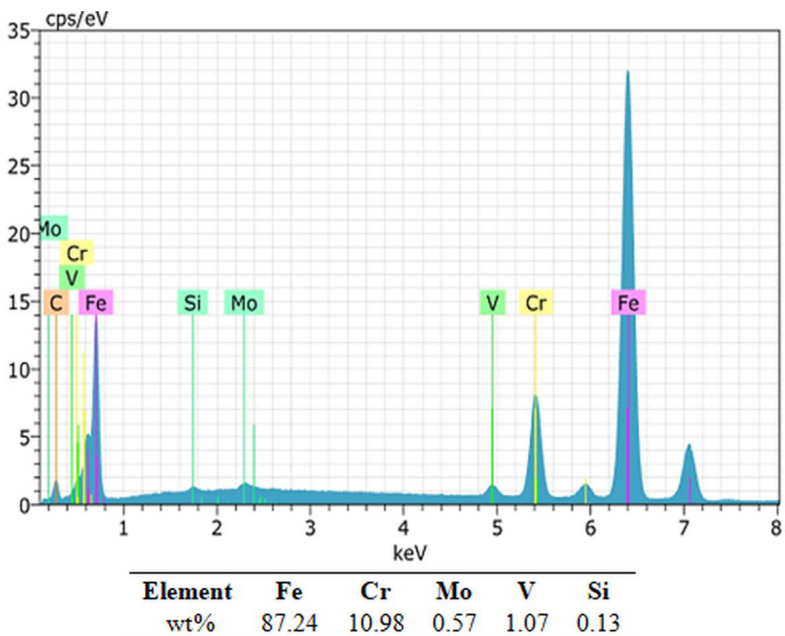
Figure 7. Spectrogram of X22CrMoV12-1 alloy in point 3.

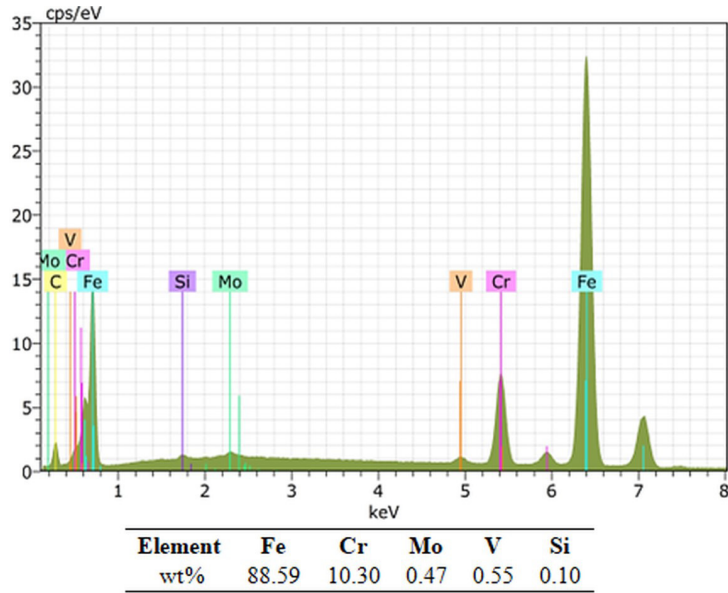| Element	Fe	Cr	Mo	V	Si
wt%	88.59	10.30	0.47	0.55	0.10

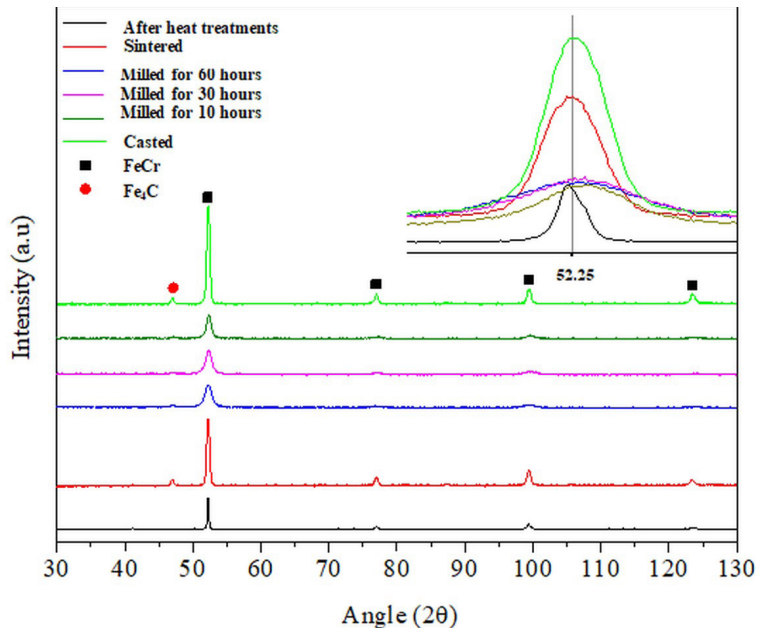**Figure 8.** Spectrogram of X22CrMoV12-1 alloy in point 4.

Figure 9. X-ray of the X22CrMoV12-1 alloy before and after milling.

FeCr and Fe_4C phases, the crystalline system corresponds to cubic.

By observing the X22CrMoV12-1 as casted, it is noted high peaks of both FeCr and Fe_4C phases. Performing the mechanical milling for 10, 30 and 60 hours, these peaks tend to reduce their intensity significantly, as a result of the refinement and amorphization of their crystalline structure. It happens because the high impact of the milling spheres against the material generates severe plastic deformations that break its crystal lattice, as the milling time increases. As a result, there is a tendency of the material to become amorphous, after advanced milling times[31-33]. After sintering, the powders return to the original crystalline structure, due to the high temperature of the process, that regenerates the original microstructure of the material[34]. Subsequently after heat treatments of quenching and tempering, it is noteworthy the dissolution of the Fe_4C phase, since that the thermal energy given by the process was sufficient for the dissolution of this phase. The absence of the VC peaks is due to a probable amorphization and consequent disappearance of this carbide, within the first hours of milling, since it presents a very small initial particles size.
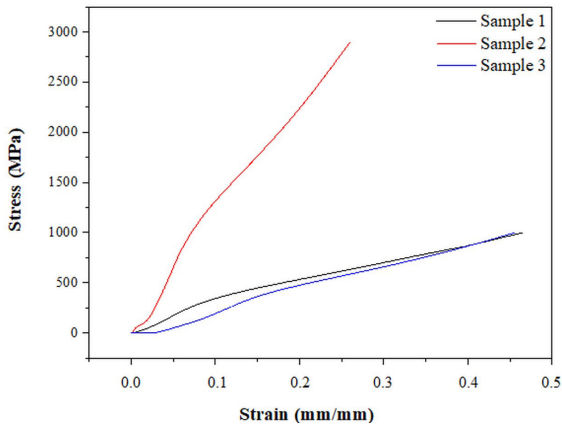
Figure 10. Stress-strain curves of X22CrMoV12-1 alloy obtained in the compressive strength test.

The stress-strain curves obtained in the compressive strength test for the best milling condition (60 hours with VC) can be seen in Figure 10. Three samples were tested, in order to achieve an average value for the elastic modulus As observed, the samples acquired good compressive strength, reaching an average elastic modulus of 11.53 GPa. In general, it is noted that sample 2 showed a different behavior than samples 1 and 3. It can happen in materials produced by PM, as a consequence of the high porosity that the samples have. Although this parameter is controlled through the pressing methods and the material particles size, sometimes some regions of the sample may end up having less or greater porosity than the average. This can generate heterogeneous mechanical results. It is known that the three samples were submitted to the same processing conditions. However, variations in their porosity were identified. Correlating the porosity with the volumetric shrinkage, a sample with a lower percentage of porosity before sintering will possibly have a higher volumetric shrinkage rate after sintering, due to the contact surface between powder particles, resulting in greater densification. On the other hand, in those samples where a higher percentage of porosity occurs before sintering, a lower volumetric shrinkage and densification rates will be observed after this heat treatment. Knowing that sample 1 presented a volumetric shrinkage of 26.1% after sintering, sample 2 of 28.4% and sample 3 of 25.9%, it is possible to attest that sample 2 presented a higher value of compressive strength due to its lower porosity, evidenced by its higher volumetric shrinkage. This parameter is great to be correlated with the inner porosity of the samples, since that the apparent porosity considers only the porosity of the samples surface.

Comparing the results obtained in Figure 10 with the elastic modulus of the casted material of 216 GPa[35], it is possible to observe that the X22CrMoV12-1 alloy with VC produced by powder metallurgy presented 5.34% of the strength of the casted material. Even this result being very below when compared to the casted material, it is potentially higher than other authors that studied steels produced by powder metallurgy, such as[36] that found a value of elastic modulus of 1.8 GPa for the AISI 52100 steel. This comparison is performed to observe how different manufacturing routes

affect the mechanical strength of the same material. These lower compressive values found for the samples produced by PM in comparison to the casted material is mainly due to the higher porosity and microstructural heterogeneity found in materials produced by PM. The greater are the number of pores, the smaller will be the particles that are in contact. Consequently, smaller will be the atomic bonds existing in the material, which implies in smaller values of mechanical strength. Besides the presence of higher porosity, other as differences in the microstructure of sintered materials in comparison to the same material produced by the traditional casting route, such as average grain size and precipitates, can influence the mechanical strength. Also, it is highlighted that the apparent porosity of 1.25% corresponds only to the superficial porosity, being the real rate of pores unknown and much higher, which decreases severely the mechanical strength of the material.

According to Xu *et al.*[37], the good mechanical results found in this research for a material processed by PM is linked to the low localized porosity in the cross-sectional area that the compressive load was applied, which consequently raised the resistance. It is also noted that the samples reached a high level of deformation without fracturing, being able to deform plastically until reaching the compressive limit of the equipment (10 tf), resulting in a disc of 3.98 mm height and 12.3 mm diameter. Although the PM is a route that generates a high percentage of pores in the microstructure of its workpieces, in this case, this technique was capable to provide an acceptable resistance to this material.

4. Conclusions

After the evaluation of X22CrMoV12-1 alloy with vanadium carbide addition submitted to powder metallurgy, the following conclusions could be made:

- It was possible to obtain powders of the X22CrMoV12-1 alloy with vanadium carbide addition, starting from its scraps.
- In the initial 10 hours of milling, particles with irregular morphology were obtained, being this morphology changed to spherical starting from 30 hours of milling, and being maintained up to 60 hours.
- With the increase in the mechanical milling times, the particles tended to increase their volume of smaller particles and decrease their volume of bigger particles.
- The milling time of 60 hours was considered the best condition, since it obtained only particles with size between 4-10 μm.
- The processes of pressing and sintering were effective, since that samples with good densification could be obtained.
- The chemical analysis and x-ray diffractogram identified the presence of two phases, corresponding to FeCr and Fe_4C, which vary with the fabrication process, milling time and heat treatment.
- As the milling time increases, there is a higher tendency of the material to become amorphous, due to the rupture of the crystalline lattice, as a

consequence of high plastic deformations induced during the milling process.

- In terms mechanical strength, it was possible to observe that the samples produced by PM obtained only 5% of the elastic modulus of the casted material. However, they presented a good result, when compared to other studies of steels produced by the same route.

- By the end of the study, the production of the X22CrMoV12-1 alloy with VC by PM was considered promising to reshape this material.

5. Acknowlegements

6. References

1. Bezhenov S. Damage evaluation of the power plants materials based on the AE model of material degradation under high-cyclic fatigue. Procedia Struct Integr. 2022;36:356-61. http://dx.doi.org/10.1016/j.prostr.2022.01.046.

2. Karakurt AS, Güneş Ü. Performance analysis of a steam turbine power plant at part load conditions. J Therm Eng. 2017;3(2):1121-8.

3. Menezes DÉS, Ralha TW, Franco LFM, Pessôa Filho PA, Fuentes MDR. Simulation and experimental study of methane-propane hydrate dissociation by high pressure differential scanning calorimetry. Braz J Chem Eng. 2018;35(2):403-14.

4. Clarke PD, Morris PF, Cardinal N, Worral MJ. Factors influencing the creep resistance of martensitic alloys for advanced power plant applications. In: Sixth International Charles Parsons Turbine Conference; 2003; Dublin, Ireland. Proceedings. Dublin: Trinity College; 2003 p. 333-45.

5. Hald J. Development status and future possibilities for martensitic creep resistant steels. In: 9th Liege Conference on Materials for Advanced Power Engineering; 2010; Liege, Belgium. Proceedings. Germany: IEK; 2010. p. 55-66.

6. Vigneron G, Vanderschaeghe A, Lecoq J. A metallurgical contribution to the industrial-development of 12% chromium martensitic steels for pressure-vessels. Int J Press Vessels Piping. 1988;32(5):389-413.

7. Klotz UE, Solenthaler C, Uggowitzer PJ. Martensitic-austenitic 9-12% Cr steels: alloy design, microstructural stability and mechanical properties. Mater Sci Eng A. 2008;476(1-2):186-94.

8. Liu Z, Gong JG, Zhao P, Zhang XC, Xuan FZ. Creep-fatigue interaction and damage behavior in 9-12%Cr steel under stress-controlled cycling at elevated temperature: effects of holding time and loading rate. Int J Fatigue. 2022;156:106684-94.

9. Ennis PJ, Czyrska-Filemonowicz A. Recent advances in creep resistant steels for power plant applications. OMNI Power Plant: operation. Maint Mater. 2002;1:1-30.

10. Ennis PJ, Czyrska-Filemonowicz A. Recent advances in creep-resistant steels for power plant applications. Sadhana. 2003;28(3-4):709-30.

11. Toro A, Sinatora A, Tanaka DK, Tschiptschin AP. Corrosion-erosion of nitrogen bearing martensitic stainless steels in seawater-quartz slurry. Wear. 2001;251(1-12):1257-64.

12. Zhang Z, Yu T, Kovacevic R. Erosion and corrosion resistance of laser cladded AISI 420 stainless steel reinforced with VC. Appl Surf Sci. 2017;410:225-40.

13. Herranz G, Romero A, Castro V, Rodríguez GP. Processing of AISI M2 high speed steel reinforced with vanadium carbide by solar sintering. Mater Des. 2014;54:934-46.

14. Suryanarayana C. Mechanical alloying: a critical review. Mater Res Lett. 2022;10(10):619-47.

15. Furlani E, Aneggi E, Leitenburg C, Maschio S. High energy ball milling of titania and titania-ceria powder mixtures. Powder Technol. 2014;254:591-6.

16. Fernandes BB, Moura C No, Ramos AS, Melo FCL, Henriques VAR. Study of Ti-7.5Si-22.5B alloys produced by powder metallurgy. Mater Res. 2014;17(3):557-64.

17. Hesse FAB, Verissimo NC, Soyama J, Bertazzoli R. High-energy ball milling of intermetallic Ti-Cu alloys for the preparation of oxide nanoparticles. Adv Powder Technol. 2021;32(12):4609-20.

18. Munir K, Biesiekierski A, Wen C, Li Y. Powder metallurgy in manufacturing of medical devices. Metallic Bio Process Med Device Manuf. 2020;1:159-90.

19. Bolzoni L. Sintering of titanium alloys: processing and properties. In: Caballero FG, editor. Encyclopedia of materials: metals and alloys. Amsterdam: Elsevier; 2022. p. 353-61. (vol. 3).

20. Akhtar S, Saad M, Misbah MR, Sati MC. Recent advancements in powder metallurgy: a review. Mater Today Proc. 2018;5(9):18649-55.

21. Jayasathyakawin S, Ravichandran M, Baskar N, Anand CC, Balasundaram R. Magnesium matrix composite for biomedical applications through powder metallurgy: review. Mater Today Proc. 2020;27:736-41.

22. Suryanarayana C. Mechanical alloying and milling. Prog Mater Sci. 2001;46(1-2):1-184.

23. Vallabh CKP, Stephens JD, Kmiecik-Lawrynowicz G, Badesha S, Sweeney M, Cetinkaya C. Predicting electrostatic charge on single microparticles. Powder Technol. 2015;286:684-96.

24. Reed JS. Principles of ceramics processing. New York: Wiley-Interscience; 1995. 688 p.

25. Chang I, Zhao Y. Advances in powder metallurgy. Amsterdam: Elsevier; 2013. 624 p.

26. Silva AGP, Alves-Júnior CA. A sinterização rápida: sua aplicação, análise e relação com as técnicas inovadoras de sinterização. Ceramica. 1998;44(290):225-32.

27. Maile K. Evaluation of microstructural parameters in 9-12% Cr-steels. Int J Press Vessels Piping. 2007;84(1-2):62-8.

28. Cipolla L, Danilesen HK, Venditti D, Di Nunzio PE, Hald J, Somers MAJ. Conversion of MX nitrides to Z-phase in a martensitic 12% Cr steel. Acta Mater. 2010;58(2):669-79.

29. Danielsen HK, Hald J. Tantalum containing Z-phase in 12%Cr martensitic steels. Scr Mater. 2009;60(9):811-3.

30. Liu F, Rashidi M, Johansson L, Hald J, Andrén HO. A new 12% chromium steel strengthened by Z-phase precipitates. Scr Mater. 2016;113:93-6.

31. Suryanarayana C. Mechanical alloying and milling. New York: CRC Press; 2004. 488 p.

32. Dias ANO, Silva A, Rodrigues CA, Melo MLNM, Rodrigues G, Silva G. Effect of high energy milling time of the aluminum bronze alloy obtained by powder metallurgy with niobium carbide addition. Mater Res. 2017;20(3):747-54.

33. Hadef F, Ans M. X-ray analysis and Rietveld refinement of ball milled Fe50Al35Ni15 powder. Surf Interfaces. 2021;26:101303-11.

34. Weeber AW, Bakker H. Amorphization by ball milling: a review. Physica B. 1988;153(1-3):93-135.

35. DIN: Deutsches Institut fur Normung. DIN EN 10269: steels and nickel alloys for fasteners with specified elevated and/or low temperature properties. Berlin: DIN; 2014.

36. Kuffner BHB, Silva G, Rodrigues CA, Rodrigues G. Study of the AISI 52100 Steel reuse through the powder metallurgy route using high energy ball milling. Mat Res. 2017;21:1-10.

37. Xu Z, Hodgson MA, Cao P. Effects of mechanical milling and sintering temperature on the densification, microstructure and tensile properties of the Fe-Mn-Si powder compacts. J Mater Sci Technol. 2016;32(11):1161-70.